ChemPubSoc Europe

DOI: 10.1002/chem.201801077

CHEMISTRY A European Journal Full Paper

Cage Compounds |*Hot Paper*|

Synthesis and Characterization of Self-Assembled Chiral $Fe^{II}_2L_3$ Cages

Bin Sun, Sandra S. Nurttila, and Joost N. H. Reek*[a]

Abstract: We present here the synthesis of chiral BINOL-derived (BINOL = 1,1′-bi-2-naphthol) bisamine and bispyridine-aldehyde building blocks that can be used for the self-assembly of novel chiral $Fe^{II}_2L_3$ cages when mixed with an iron(II) precursor. The properties of a series of chiral cages were studied by NMR and circular dichroism (CD) spectroscopy, cold-spray ionization MS, and molecular modeling. Upon formation of the M_2L_3 cages, the iron corners can adopt various isomeric forms: *mer*, *fac*-Δ, or *fac*-Λ. We found that the coordination geometry around the metal centers in **R-Cages 1** and **2** were influenced by the chiral BINOL backbone only to a limited extent, as a mixture of cages was formed with *fac* and *mer* configurations at the iron corners. However, single cage species (*fac*-**RR-Cage** and *fac*-**RS-Cage**) that are enantiopure and highly symmetric were obtained by generating these chiral M_2L_3 cages by using the bispyridine-aldehyde building blocks in combination with chiral amine moieties to form pyridylimine ligands for coordination to iron. Next to consistent NMR spectra, the CD spectra confirm the configurations *fac*-(Λ,Λ) and *fac*-(Δ,Δ) corresponding to **RR-** and **RS-Cage**, respectively.

Introduction

The field of self-assembled cages has been developing rapidly, and several applications have been explored, including catalysis.[1] The use of metal–ligand coordination is particularly powerful for the generation of cages, as these interactions are directional and can be rather strong, yet sufficiently dynamic to allow the thermodynamically most stable species to be formed.[1e,f,2] The use of chiral cages for enantioselective catalysis, controlled by the second coordination sphere defined by the cage, is a virtually unexplored field. In fact, the number of chiral metallocages is rather limited. In view of our interest in catalysis in confined spaces,[3–12] which can result in unusual selectivity and activity,[1e,g,2k,13] we were interested to learn whether specific reactions could be performed in an enantioselective fashion as a result of the fact that the reaction takes place in a chiral cage. Analysis of currently available chiral cages showed that such cages could be inherently chiral or could be chiral because of the application of chiral building blocks, that is, the vertices or the edges connecting coordination complexes. Raymond demonstrated that chiral cages could be prepared by the use of chiral templates, which could be displaced by non-chiral analogues after cage formation.[14] If chiral cages are generated by using enantiopure building blocks, their effect on the coordination stereochemistry should be considered.[15] This was thoroughly investigated by the Nitschke group, who introduced a very powerful subcomponent self-assembly strategy based on pyridylimine ligands.[16] They reported that for some systems the stereoselectivity at the coordination complexes at the corners of their tetrahedral cage was controlled by stereochemical communication by the chirality at either the vertices or the ligands used for coordination.[17–19] For example, during the formation of the coordination centers in $Fe^{II}_4L_4$ cages, additional chiral moieties were introduced to force the metal centers to adopt a single stereoisomer, which led to enantiopure cage structures. In some examples, the chirality of the cage remained even after exchange of the chiral auxiliaries by achiral analogues.[18] This was the case only for cages that were relatively rigid, as racemization under ambient conditions was prevented. This method has been studied for M_4L_6-type cages by various groups, but for M_2L_3-type cages this method remains unexplored. The use of 1,1′-bi-2-naphthol (BINOL) as a chiral scaffold is interesting, as it has successfully been applied as a versatile chiral element in asymmetric catalysis, and as such, a diverse set of building blocks is available.[20] BINOL-based building blocks have also been investigated as chiral units for the construction of supramolecular chiral structures.[21–26] In this contribution, we report BINOL-based building blocks for the construction of $Fe^{II}_2L_3$-type cages by using the typical Nitschke subcomponent self-assembly strategy. Various $Fe^{II}_2L_3$ cages were prepared, and within this series, the extent to which the chiral information at the BINOL building blocks

[a] *B. Sun, S. S. Nurttila, Prof. Dr. J. N. H. Reek*
Homogeneous, Bioinspired and Supramolecular Catalysis
van 't Hoff Institute for Molecular Sciences, University of Amsterdam
Science Park 904, 1098 XH Amsterdam (The Netherlands)
E-mail: j.n.h.reek@uva.nl

Supporting Information and the ORCID identification number(s) for the author(s) of this article can be found under: https://doi.org/10.1002/chem.201801077.

could be transferred to the coordination centers was evaluated. We conclude that enantiopure single-isomer cages only form if, next to the BINOL building blocks, chiral amines are used to steer the chirality at the coordination complexes around iron.

Results and Discussion

We first designed and synthesized BINOL derivative **R-Ligand 1**, with two phenylamine terminating groups required for the coordination chemistry typically applied by Nitschke for the self-assembly of cages. **R-Ligand 1** was synthesized from enantiomerically pure (*R*)-2,2′-bis(methoxymethoxy)-3,3′-diiodo-1,1′-binaphthalene (**1**) in four steps in 49% overall yield (Figure 1) and was fully characterized by NMR spectroscopy and HRMS. The *S* isomer was prepared by using a similar route.

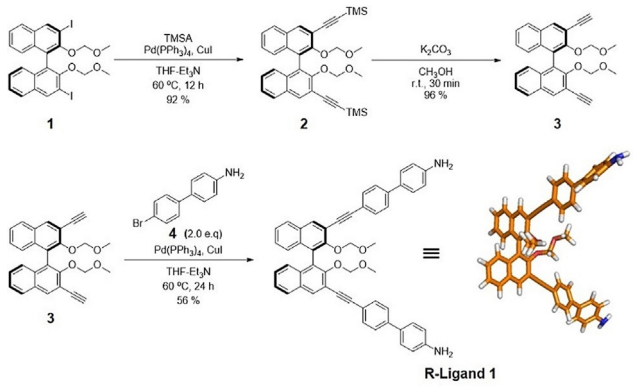

Figure 1. Synthesis of BINOL-based diamine **R-Ligand 1**. TMSA = trimethylsilylacetylene.

Cage formation was achieved by mixing 2-formylpyridine, **R-Ligand 1**, and iron(II) bis(trifluoromethane)sulfonimide [$Fe(NTf_2)_2$] in a 6:3:2 ratio in dry acetonitrile under an atmosphere of nitrogen (Figure 2a). An intensely colored purple solution formed immediately, and after the mixture was heated at 65 °C for 12 h, an air-stable solid was isolated after precipitation by the addition of diethyl ether. The isolated solid was dark purple in color, which is in line with the formation of a charge-transfer complex typical for these types of low-spin Fe^{II} pyridylimine complexes. **S-Cage 1** was obtained by using a similar method.

Cage formation was confirmed by a combination of spectroscopic techniques, including MS analysis and NMR spectroscopy. The ^{1}H NMR signals are generally relative sharp, which is indicative of the formation of a well-defined discrete structure (Figure 2b). The signals for the BINOL core of the cage are shifted significantly relative to the corresponding signals for free **R-Ligand 1**. Indicative of the formation of an imine are the signals at approximately $\delta = 8.6$–8.9 ppm (in the red dashed circle), which were assigned with the help of 2D ^{1}H COSY NMR (see the Supporting Information, Figure S15). The presence of multiple imine signals suggests the formation of various cage isomers. The sizes of the cages in solution were determined by

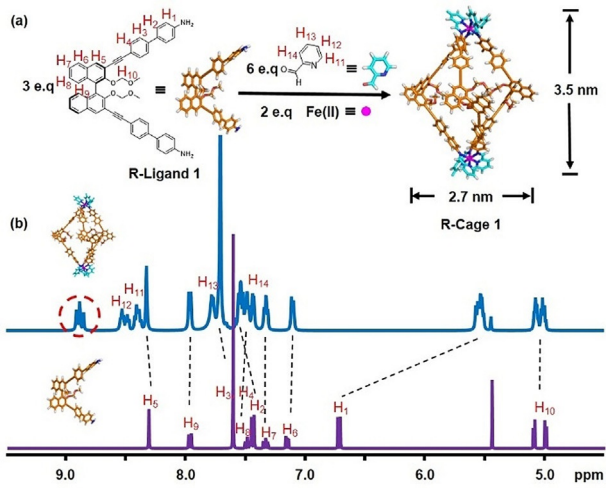

Figure 2. a) Self-Assembly of **R-Cage 1**. b) Parts of the ^{1}H NMR spectra of **R-Cage 1** (top) and **R-Ligand 1** (bottom) (400 MHz, CD_3CN, 298 K). The modeled structure of **R-Cage 1** is displayed.

diffusion-ordered NMR spectroscopy (DOSY), displaying a narrow band around $\log D = -9.22$ m^2 s^{-1}, which is in line with the formation of self-assembled cages that are 2.5 nm in size (Figure S59). This value is in agreement with the diameter of **R-Cage 1** obtained by molecular modeling. As only one band is observed, the various cage isomers are of the same size, and this is further confirmed by cold-spray ionization (CSI) MS.

CSI-MS analysis of an acetonitrile solution of **R-Cage 1** resulted in a clean spectrum (Figure 3) with a clear set of signals (charged states 2+, 3+, and 4+) belonging to the same species. These signals are consistent with the molecular weight of **R-Cage 1** with different numbers of NTf_2^- counterions, as expected for these different charges. For each charged state, the experimental and simulated isotope pattern curves match perfectly (Figure S39), and this is displayed in the inset of Figure 3 for the 3+ charged species. Clearly, the experimental data are

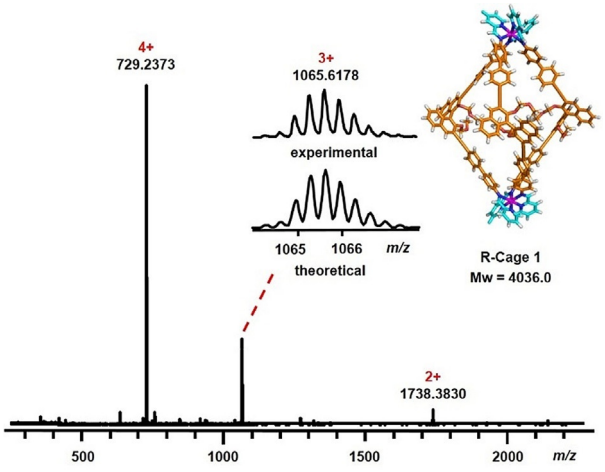

Figure 3. CSI-MS of **R-Cage 1**, with the inset showing the theoretical and experimental isotopic distributions of the 3+ signal.

consistent with a cage structure with a molecular weight of 4036.6 Da, corresponding to the composition $Fe_2L_3(NTf_2)_4$.

Next, the chirality of cages **R-Cage 1** and **S-Cage 1** was studied by circular dichroism (CD). The spectra of the *R* and *S* isomers of the ligands as well as the cages are perfect mirror images (Figures S43 and S45), and therefore, only the *R* isomer is described in the following text. The CD spectra of both the ligand and the complex show split-type Cotton effects (Figure 4). Relative to the signals in the CD spectrum of **R-Ligand 1**, those in the CD spectrum of **R-Cage 1** are more intense as a result of the higher concentration of the chiral building block with significant signals at approximately $\lambda =$ 240, 280, 320, and 350 nm, which can be attributed to the π–π^* transitions in the organic backbones, also corresponding to the bands observed in the UV/Vis spectra.[27,28] The signal centered at $\lambda = 320$ nm in the curve of **R-Cage 1** is particularly intense, and this is in line with the new absorbance band at $\lambda =$ 280 nm in the UV/Vis spectrum. Importantly, there is no distinct signal in the CD spectrum of the cage in the region between $\lambda = 500$ and 600 nm, whereas the UV/Vis spectrum does show a weak absorption as a result of a metal-to-ligand charge-transfer (MLCT) band. As this MLCT band in the UV/Vis spectrum is attributed to the metal complexes of the cage[28] and does not show a CD effect in this region, there is no overall chirality of the metal centers in the cage; this is in line with the NMR spectra and suggests that various isomers are formed.

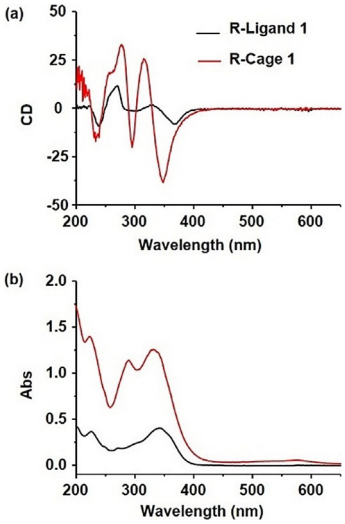

Figure 4. a) CD spectra and b) UV/Vis spectra of **R-Ligand 1** and **R-Cage 1**. All the spectra were recorded in acetonitrile at a concentration of 0.05 mM.

Generally, these pyridylimine-based multicomponent octahedral coordination complexes can form with facial (*fac*) or meridional (*mer*) geometry in both the Λ and Δ enantiomeric forms. For mononuclear complexes of this type, usually racemic mixtures of the *fac* and *mer* isomers form in ratios that depend on the substituents on the pyridine or amine derivate.[28–30] For cages that have two metal centers, in principle, complicated mixtures of cage isomers could form; however, the relatively simple ^{1}H NMR spectra suggest the presence of a limited number of isomers. For interpretation, the region of the ^{1}H NMR spectra in which the imine signals resonate is of particular interest, as the *fac* and *mer* conformations give distinctly different signals. The facial conformation is highly symmetric and, therefore, gives one singlet for the imine protons, whereas for the meridional coordination complex the imine protons reside in different chemical and magnetic environments and, as a result, produce three separate singlets. A mixture of cages with *mer*-(Λ,Λ), *mer*-(Δ,Δ), and *mer*-(Λ,Δ) configurations at the metal corners, therefore, should lead to 12 signals in the imine region. A mixture of cages with *fac*-(Λ,Λ), *fac*-(Δ,Δ), and *fac*-(Λ,Δ) configurations is expected to give four different signals, which is consistent with the experimental NMR spectrum. In line with this, molecular modeling of all different cages shows that cages with the *mer* configuration at either one of the metal centers result in structures with twisted ligands, which are higher in energy (Figure S50). As such, we prudently conclude that during the formation of the cage the chiral building blocks control the configuration but not the chirality at the metal coordination sites, as a mixture of cages with the *fac*-(Λ,Λ), *fac*-(Δ,Δ), and *fac*-(Λ,Δ) configurations is formed, in line with the reported examples.[29,31]

As the chirality at the metal center is not influenced by the chirality of the BINOL moiety, we sought other ways to control the chirality eventually to form cages in enantiopure form. Several factors have been reported to affect the chirality of metal complexes in coordination cages, including the coordination preference of the metal, the geometric and steric properties of the ligands, and experimental conditions such as the metal–ligand ratio and concentration in the specific solution.[5e] The most direct way to the selective formation of either *fac*-(Λ) or *fac*-(Δ) metal centers is by the introduction of chiral groups at the ligands close to the metal center.[18,32,33] Therefore, we decided to design and synthesize **R-Ligand 2** (Figure 5), also based on a BINOL core but with formylpyridine functional groups that would allow formation of chiral ligands after condensation with chiral amines. Both the *R* and *S* isomers of **2** were successfully synthesized through the coupling reaction between compound **3** and formylpyridine **5**. The new building block was obtained in 56% yield and was fully characterized by a combination of techniques (Figures S7–S12).

We first studied cage formation by using achiral benzylamine (Figure 6a). A mixture of benzylamine, **R-Ligand 2**, and $Fe(NTf_2)_2$ in a 6:3:2 ratio in dry acetonitrile was stirred at 65 °C

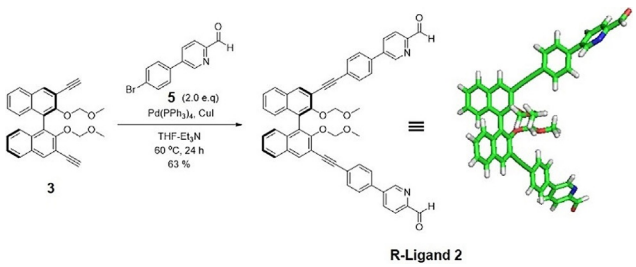

Figure 5. Synthesis of BINOL-based diformylpyridine **R-Ligand 2**.

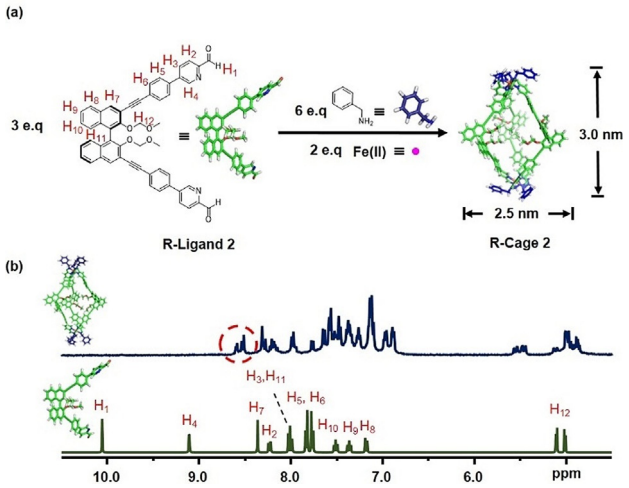

Figure 6. a) Self-assembly of **R-Cage 2**. b) Parts of the ^{1}H NMR spectra of **R-Cage 2** (top) and **R-Ligand 2** (bottom) (400 MHz, CD_3CN, 298 K). The modeled structure of **R-Cage 2** is also displayed.

for 12 h under an inert atmosphere. After precipitation with diethyl ether, a dark-purple solid was collected by centrifugation. The compound was analyzed by CSI-MS and NMR spectroscopy, which confirmed the formation of **R-Cage 2**. The CSI mass spectrum displays signals at $m/z = 729$, 1065, and 1738, which is in line with the formation of $Fe^{II}_2L_3(NTf_2)_4$ (Figure S40). Also, the NMR spectroscopy data (^{1}H NMR, DOSY) confirm the formation of **R-Cage 2** (Figures S19 and S60). The presence of multiple imine signals and multiple sets of signals for the CH_2 group of benzylamine around $\delta = 5.5$ ppm reveals again the formation of a mixture of cages similar to **R-Cage 1** (Figure 6b).[28]

The CD spectra of acetonitrile solutions of 0.05 mM **R-Ligand 2** and 0.05 mM **R-Cage 2** were measured in a fashion similar to that of **R-Ligand 1** and its cage (Figure 7). The signals of the cage are larger than those of the free ligand, for example, between $\lambda = 200$ and 300 nm, as a result of a higher concentration of the BINOL building block, as the M_2L_3 cage contains 3 equivalents. Comparing the spectra of the cage and ligand, the signals between $\lambda = 300$ and 400 nm are also slightly different in shape. Most importantly, there is a small positive signal centered at $\lambda = 550$ nm corresponding to the MLCT band of the iron complex, which suggests that in this cage the iron complex is not formed in racemic form. Apparently, there is some induction of chirality by the BINOL building block. The NMR spectra, however, show that various isomeric forms of the cage are formed and that they differ in coordination at the iron centers. Therefore, also for this cage, in the absence of chiral ligands around the iron center, the self-assembly does not lead to the formation of a single cage species in enantiopure form.

Next, we studied the formation of cages by using chiral amines as the second chiral component, generating systems in which the ligands around the iron complexes are also chiral. The self-assembled **RR-Cage** was formed by stirring **R-Ligand 2** with $Fe(NTf_2)_2$ and (*R*)-α-phenylethylamine (in a ratio of 3:2:6) in acetonitrile under an inert atmosphere, which immediately resulted in the formation of an intense purple solution. After stirring at 65 °C for 12 h, the cage was isolated as a precipitate after adding an excess amount of diethyl ether and was collected as a dark-purple solid. CSI-MS analysis confirmed the formation of the **RR-Cage** with predominant signals at $m/z =$ 1822, 1121, and 771, which are in line with the predicted cage signals of charges 2+, 3+, and 4+ (Figure 8). The isotopic distribution for each charged state accurately matches the theoretical simulated spectrum (Figure S41). The molecular weight, as determined from the MS experiment, is 4204.8 Da, which is consistent with the expected formation of the $Fe^{II}_2L_3(NTf_2)_4$ cage. The **RS-Cage** was prepared in a similar fashion, and the MS data are also identical (Figure S41).

The ^{1}H NMR spectra of both the **RR** and **RS-Cage** (Figure 9a) also confirm the formation of the cages, as all signals of the protons of the BINOL cores and the formylpyridine rings are shifted with respect to the signals of the free building blocks. Importantly, for these cages the signals corresponding to the

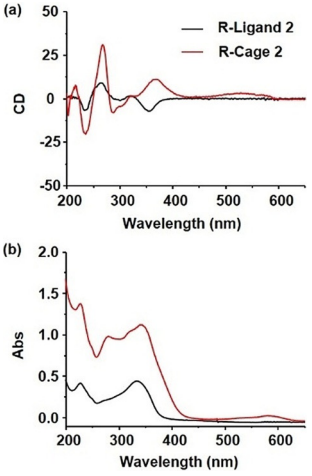

Figure 7. a) CD spectra and b) UV/Vis spectra of **R-Ligand 2** and **R-Cage 2**. All spectra were recorded in acetonitrile at a concentration of 0.05 mM.

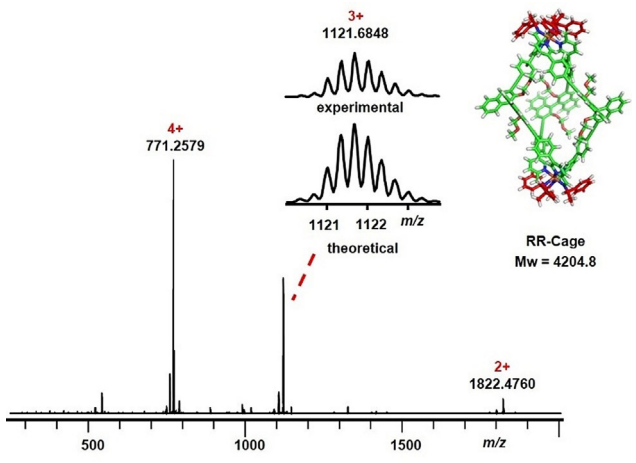

Figure 8. CSI-MS of **RR-Cage**, with the inset showing the theoretical and experimental isotopic distributions of the 3+ signal.

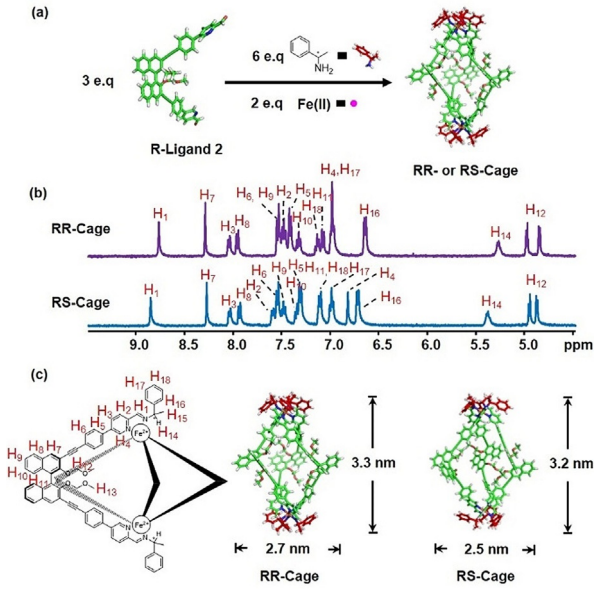

Figure 9. a) Self-Assembly of **RR-Cage** and **RS-Cage**. b) Parts of the ^{1}H NMR spectra of **RR-Cage** (top) and **RS-Cage** (bottom) (400 MHz, CD_3CN, 298 K). c) Modeled structures of **RR-Cage** and **RS-Cage**.

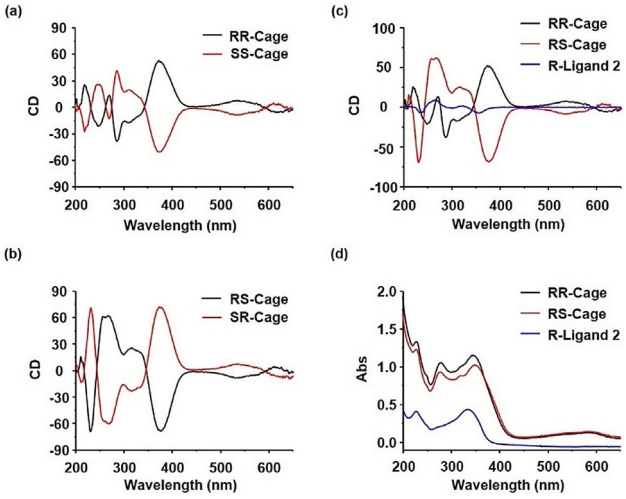

Figure 10. a–c) CD spectra of **RR** and **SS-Cage**, **RS** and **SR-Cage**, and **R-Ligand 2**. d) UV/Vis spectra of **RR-Cage**, **RS-Cage**, and **R-Ligand 2**. All spectra were recorded in acetonitrile at a concentration of 0.05 mM.

imine protons appear as a single singlet, which is in line with the formation of a single enantiomeric form of the cage, with facial coordination geometry around the iron metal center. The ^{1}H NMR spectra of **RR-Cage** and **RS-Cage** are similarly simple and are only slightly different, as expected for diastereomeric compounds. For example, the signal of the imine proton is somewhat shifted, which indicates that these diastereoisomers have slightly different overall structures. Interestingly, the DOSY spectra show narrow bands for both **RR-Cage** and **RS-Cage**, and the small difference in diffusion indicates the small difference in size (log $D = -9.38$ and -9.32 $m^2 s^{-1}$, respectively; Figures S61). In addition, in the NOESY spectra (Figures S28 and S32), cross peaks between protons of the phenyl rings of the amine and the formylpyridine rings are observed, and this is indicative of π-stacking interactions between these groups in both **RR-Cage** and **RS-Cage**, in line with the descriptions of reported analogues.[28,30] The molecular models presented in Figure 9b also show that these groups are in close proximity. All data show that the use of chiral amines in the formation of these novel M_2L_3 self-assembled cages results in the formation of discrete, highly symmetric structures, with a single coordination mode around iron leading to a single cage species. The cages based on the *S* enantiomeric form of the BINOL building block were also prepared, and they show similar spectroscopic data.

All four diastereomeric cages were studied by CD spectroscopy. The spectra of **RR-** and **SS-Cage** and those of **RS-** and **SR-Cage** are perfect mirror images, as expected for enantiomeric pairs (Figure 10). For clarity, we will focus here on **RR-** and **RS-Cage**. The CD signals between $\lambda = 220$ and 300 nm correspond to the π–π* transitions of the organic backbones. The apparent opposite bands at $\lambda = 320$m and 370 nm can be assigned to the presence of the chiral amines, as they are absent in the spectra of **R-Cage 2**. Importantly, there are two clear bands at approximately $\lambda = 550$ and 600 nm, which are in the MLCT area, in line with the formation of enantiopure iron complexes.[28] Also, this band shows a perfect mirror image for the two enantiomeric forms of the cage. This suggests that the complexes of one cage are of the same chirality, as if the two metal centers were formed in opposite configurations, the CD signals should cancel out. These CD spectra together with the highly symmetric NMR spectra, with a single signal for the imine, indicate that these cages form as single species in enantiopure form. Comparing the data of our new cages with those reported for monoiron(II) complexes [27,28] or the tetrahedral capsules of Nitschke[18] suggests that the chiral amine dictates the chirality at the metal center. If an (*S*)-amine is used for cage formation, the configuration can be assigned to *fac*-Δ, and the use of the (*R*)-amine leads to the *fac*-Λ configuration. In summary, diastereomeric **RR-Cage** forms as *fac*-(Λ,Λ) and **RS-Cage** forms as *fac*-(Δ,Δ).

Initial binding studies were performed to probe the properties of these new cages to act as host molecules. We explored various different guest molecules, including BINOL, limonene, and glucose. These compounds were previously demonstrated to bind into the Nitschke cages, although for the current experiments acetonitrile was used instead of water as the solvent. Unfortunately, none of the explored guests had significant affinity for the cages under these conditions (see the Supporting Information), which suggests that for the selective binding of guests with these cages we have to move to water-soluble analogues or install functional groups to provide complementary interactions with the potentials guests.

Conclusions

In conclusion, we prepared various BINOL-based building blocks for the subcomponent self-assembly of $[Fe_2L_3]$-typed cages. The amine-functionalized BINOL building block in com-

bination with 2-formylpyridine resulted in a mixture of $[Fe_2L_3]$ cages, in which the iron complexes had a *fac* geometry. The isomers differed in chirality at the metal complexes, which showed that the chirality of the BINOL building block did not steer the chirality at the metal corners during cage formation. The same held true for cages that were constructed from the aldehyde-functionalized building blocks that were combined with achiral amines. Only if this building block was used in combination with a chiral amine did the subcomponent self-assembly result in enantiopure $[Fe_2L_3]$ cages. These enantiopure subcomponent $[Fe_2L_3]$ cages that contain chiral BINOL groups provide an interesting scaffold for cage-controlled enantioselective catalysis. Installation of catalyst function could be foreseen by the previously established template-ligand approach[3,5,9] or by converting the BINOL building blocks into a ligand scaffold, which in both cases would involve the preparation of new building blocks, as the BINOL groups in the current cages cannot be deprotected. Work along these lines is in progress in our laboratories.

Experimental Section

General information

All reactions were performed under an atmosphere of N_2 by using standard Schlenk techniques unless otherwise stated. All reagents were purchased from Sigma Aldrich Chemie and Fluorochem and were used without further purification. All solvents were distilled by using standard procedures. All NMR spectra were recorded with Bruker Avance 400 MHz and 500 MHz NMR spectrometers in $CDCl_3$ or CD_3CN. Mass spectra were collected with an AccuTOF LC, JMS-T100LP mass spectrometer (JEOL, Japan) equipped with a CSI source (JEOL, Japan). Detection was in positive-ion mode. The ion source temperature was held at 30 °C, and the spray temperature was held at −20 °C. UV/Vis spectra were recorded with a Shimadzu UV-2000 spectrophotometer in a 10 mm quartz cuvette. CD spectra were recorded with the Olis DSM 1000 CD instrument in a 10 mm quartz cuvette at a concentration of 0.05 mM.

Synthesis of the ligands

(*R*)- and (*S*)-2,2′-Bis(methoxymethoxy)-3,3′-diiodo-1,1′-binaphthalene (**1**) and 2-(4-bromophenyl)-4,4,5,5-tetramethyl-1,3,2-dioxaborolane were synthesized according to reported methods,[34,35] and the spectroscopic data were similar to those reported in the literature. All *S* isomers were synthesized by using similar methods and showed similar properties.

Compound 2: This compound was synthesized according to a modified literature procedure.[34] A 100 mL Schlenk flask was charged with **1** (1.35 g, 2.16 mmol), tetrakis(triphenylphosphine) palladium (0.125 g, 5 mol%), and copper iodide (0.02 g, 5 mol%) wand was then degassed and backfilled with nitrogen (3×). THF (20 mL) and Et_3N (20 mL) were injected into the mixture. The mixture was stirred at 60 °C for 30 min. Then, TMSA (1.21 mL, 8.60 mmol) was injected by syringe. After stirring at 60 °C for another 12 h, the mixture was cooled to room temperature, and the solvent was removed under vacuum. The residue was purified by column chromatography on silica gel (dichloromethane/hexanes = 1:1, *v/v*) to give **2** (1.12 g, 92%) as a white foam solid. ^{1}H NMR (400 MHz, $CDCl_3$, 298 K): δ = 8.15 (s, 2H), 7.81 (d, J = 6.0 Hz, 2H) 7.39 (dd, J = 6.0, 6.5 Hz, 2H), 7.27 (dd, J = 6.0, 6.5 Hz, 2H), 7.15 (d, J = 6.5 Hz, 2H), 5.17 (d, J = 5.5 Hz, 2H), 4.86 (d, J = 5.5 Hz, 2H), 2.45 (s, 6H), 0.24 ppm (s, 18H); ^{13}C NMR (100 MHz, $CDCl_3$): δ = 153.5, 135.0, 134.0, 130.3, 127.6, 127.4, 126.7, 125.9, 125.6, 117.6, 102.0, 99.2, 98.8, 56.1, 0.08 ppm.

Compound 3: This compound was synthesized according to a modified literature method.[34] Compound **2** (1.22 g, 2.16 mmol) was dissolved in methanol (20 mL) and then potassium carbonate (1.49 g, 10.8 mmol) was added. The mixture was stirred at room temperature for 30 min, and the reaction was monitored by TLC. Upon completion of the reaction, potassium carbonate was removed by filtration. The filtrate was concentrated, and the crude product was purified by column chromatography on silica gel (dichloromethane/hexanes = 2:1, *v/v*) to give **3** (0.87 g, 96%) as a white foam solid. ^{1}H NMR (400 MHz, $CDCl_3$, 298 K): δ = 8.20 (s, 2H), 7.83 (m, 2H), 7.43 (m, 2H), 7.31 (m, 2H), 7.19 (m, 2H), 5.08 (d, J = 6.0 Hz, 2H), 4.89 (d, J = 6.0 Hz, 2H), 3.33 (s, 2H), 2.53 ppm (s, 6H); ^{13}C NMR (100 MHz, $CDCl_3$, 298 K): δ = 153.4, 135.4, 134.1, 130.2, 127.7, 127.6, 126.6, 125.9, 125.7, 116.4, 99.0, 81.7, 80.7, 56.2 ppm.

Compound 4: 4-Bromoaniline (1.72 g, 10.0 mmol), 2-(4-bromophenyl)-4,4,5,5-tetramethyl-1,3,2-dioxaborolane (1.41 g, 5.0 mmol), bis(triphenylphosphine)palladium chloride (0.18 g, 5.0 mol%), and potassium carbonate (4.15 g, 30.0 mmol) were transferred into a 200 mL Schlenk flask. Under a nitrogen atmosphere, toluene (100 mL) and H_2O (15 mL) were added, and the mixture was stirred at 90 °C for 12 h. After cooling to room temperature, the organic layer was separated, and the aqueous layer was extracted with dichloromethane (3×100 mL). The combined organic layer was washed with brine and dried with anhydrous Na_2SO_4, and then the solvent was removed. The residue was purified by silica gel column chromatography (dichloromethane/hexanes = 3:1, *v/v*) to give **4** (0.81 g, 66%) as a yellow solid. ^{1}H NMR (400 MHz, $CDCl_3$, 298 K): δ = 7.50 (d, J = 8.2 Hz, 2H), 7.38 (t, J = 8.2 Hz, 4H), 6.78–6.71 (m,2H), 3.75 ppm (s, 2H); ^{13}C NMR (100 MHz, $CDCl_3$): δ = 140.10, 131.81, 128.78, 128.07, 127.88, 126.53, 120.42, 115.92 ppm; HRMS: *m/z*: calcd for $[C_{12}H_{10}NBr]^+$: 246.9997; found: 246.9993.

R-Ligand 1: A 50 mL Schlenk flask was charged with **3** (0.32 g, 0.76 mmol), **4** (0.38 g, 1.52 mmol), tetrakis(triphenylphosphine)palladium (44.0 mg, 5 mol%), and copper iodide (8.0 mg, 5 mol%). After degassing and backfilling with nitrogen (3×), THF (10 mL) and Et_3N (10 mL) were injected into the flask. After stirring at 60 °C for 24 h, the mixture was cooled to room temperature. The mixture was filtered through Celite, and thereafter the solvent was removed. The residue was purified by silica gel column chromatography (dichloromethane/ethyl acetate = 10:1, *v/v*) to give **R-Ligand 1** (655 mg, 56%) as a brown foam. ^{1}H NMR (400 MHz, CD_3CN, 298 K): δ = 8.32 (d, J = 0.7 Hz, 2H), 7.99–7.95 (m, 2H), 7.61 (s, 9H), 7.49 (ddd, J = 8.2, 6.8, 1.2 Hz, 2H), 7.47–7.42 (m, 4H), 7.34 (ddd, J = 8.3, 6.8, 1.3 Hz, 2H), 7.16 (dt, J = 8.6, 0.9 Hz, 2H), 6.73 (d, J = 8.6 Hz, 4H), 5.10 (d, J = 5.9 Hz, 2H), 5.00 (d, J = 5.8 Hz, 2H), 4.32 (s, 5H), 2.60 ppm (s, 6H); ^{13}C NMR (100 MHz, $CDCl_3$, 298 K): δ = 153.1, 146.4, 141.3, 134.2, 133.8, 132.0, 130.5, 128.0, 127.7, 127.3, 126.7, 126.3, 126.0, 125.6, 120.9, 117.6, 115.5, 99.0, 94.2, 86.9, 56.2 ppm; HRMS: *m/z*: calcd for $[C_{52}H_{40}N_2O_4]^+$: 756.2988; found: 756.2972. (^{1}H NMR was recorded in CD_3CN to compare easily with the cage)

Compound 5: 5-Bromo-2-pyridinecarboxaldehyde (0.62 g, 3.33 mmol), 2-(4-bromophenyl)-4,4,5,5-tetramethyl-1,3,2-dioxaborolane (1.41 g, 5.0 mmol), Pd(dppf)Cl_2 [0.14 g, 5.0 mol%; dppf = 1,1′-bis(diphenylphosphino)ferrocene], and potassium carbonate (4.15 g, 30.0 mmol) were added into a 200 mL Schlenk flask. Under a nitrogen atmosphere, dioxane (120 mL) and H_2O (15 mL) were added, and the mixture was stirred at 80 °C for 24 h. After cooling to room temperature, the mixture was poured into dichloromethane (100 mL) and water (100 mL). The organic layer was sepa-

rated, and the aqueous layer was extracted with dichloromethane (3×100 mL). The combined organic layer was washed with brine (3×100 mL) and was then dried with anhydrous Na_2SO_4. The solvent was removed. The residue was purified by silica gel column chromatography (dichloromethane/ethyl acetate = 20:1, *v/v*) to give **5** (0.51 g, 58%) as a yellow solid. ^{1}H NMR (400 MHz, $CDCl_3$, 298 K): δ = 10.13 (s, 1H), 8.98 (s, 1H), 8.04 (d, J = 2.9 Hz, 2H), 7.71–7.63 (m, 2H), 7.57–7.47 ppm (m, 2H); ^{13}C NMR (100 MHz, $CDCl_3$, 298 K): δ = 193.0, 151.9, 148.5, 139.7, 135.6, 135.2, 132.7, 129.1, 123.9, 122.0 ppm; HRMS: *m/z*: calcd for $[C_{12}H_8NOBr]^+$: 260.9789; found: 260.9788.

R-Ligand 2: A 50 mL Schlenk flask was charged with **3** (0.63 g, 1.50 mmol), **5** (0.80 g, 3.00 mmol), tetrakis(triphenylphosphine) palladium (87.0 mg, 5 mol%), and copper iodide (15.0 mg, 5 mol%). After degassing, THF (10 mL) and Et_3N (10 mL) were injected into the flask. After stirring at 60 °C for 24 h, the mixture was cooled to room temperature. The mixture was filtered through Celite, and thereafter the solvent was removed. The residue was purified by silica gel column chromatography (dichloromethane/ethyl acetate = 10:1, *v/v*) to give **R-Ligand 2** (362 mg, 63%) as a yellow foam solid. ^{1}H NMR (400 MHz, CD_3CN, 298 K): δ = 10.06 (d, J = 0.8 Hz, 2H), 9.11 (dd, J = 2.3, 0.9 Hz, 2H), 8.36 (s, 2H), 8.23 (ddd, J = 8.2, 2.3, 0.9 Hz, 2H), 8.01 (dd, J = 8.9, 7.9 Hz, 4H), 7.86–7.80 (m, 4H), 7.80–7.74 (m, 4H), 7.51 (ddd, J = 8.1, 6.8, 1.2 Hz, 3H), 7.37 (ddd, J = 8.3, 6.8, 1.3 Hz, 3H), 7.18 (d, J = 8.5 Hz, 2H), 5.10 (d, J = 5.8 Hz, 2H), 5.01 (d, J = 5.9 Hz, 2H), 2.61 ppm (s, 5H);^{13}C NMR (100 MHz, $CDCl_3$, 298 K): δ = 193.0, 153.1, 151.8, 148.6, 139.9, 136.5, 135.2, 134.6, 134.0, 132.5, 130.4, 128.0, 127.8, 127.6, 127.5, 126.7, 126.0, 125.8, 124.3, 122.0, 117.1, 99.1, 93.1, 88.6, 56.3 ppm; HRMS: *m/z*: calcd for $[C_{52}H_{36}N_2O_6]^+$: 784.2573; found: 784.2565. (^{1}H NMR was recorded in CD_3CN to compare easily with the cage)

General procedure for cage synthesis

A 10 mL Schlenk flask was charged with the ligand (3.0 equiv.) and $Fe(NTf_2)_2$ (2.0 equiv.). After degassing and filling with nitrogen, freshly distilled CH_3CN (2.0 mL) was added. The whole system was sonicated to enhance dissolution of the ligand. 4-Formylpyridine (6.0 equiv.), benzylamine (6.0 equiv.), or enantiopure α-phenylethylamine (6.0 equiv.) was injected, and an intense purple solution was formed immediately. The solution was stirred at 65 °C for 12 h. After cooling to room temperature, the dark-purple solution was transferred into dried diethyl ether (30 mL) through a syringe filter. After centrifugation, a dark-purple solid was collected and dried under vacuum.

R-Cage 1: Following the general procedure, **R-Ligand 1** (22.7 mg, 0.03 mmol), $Fe(NTf_2)_2$ (12.3 mg, 0.02 mmol), and 4-formylpyridine (6.43 mg, 0.06 mmol) were added in order. **R-Cage 1** was isolated as a dark-purple solid (30.3 mg, 75%). ^{1}H NMR (400 MHz, CD_3CN, 298 K): δ = 8.91 (s, 1H), 8.89 (s, 1H), 8.85 (s, 1H), 8.53 (t, J = 6.8 Hz, 2H), 8.49 (t, J = 7.0 Hz, 2H), 8.42 (d, J = 7.6 Hz, 3H), 8.33 (s, 3H), 7.96 (d, J = 8.3 Hz, 4H), 7.79 (d, J = 6.3 Hz, 6H), 7.71 (s, 12H), 7.59–7.51 (m, 8H), 7.49 (t, J = 7.5 Hz, 4H), 7.43 (d, J = 5.6 Hz, 4H), 7.33 (t, J = 7.7 Hz, 4H), 7.11 (d, J = 8.7 Hz, 3H), 5.61–5.48 (m, 6H), 5.07 (td, J = 8.7, 7.4, 4.3 Hz, 4H), 5.04–4.95 (m, 4H), 2.64 (s, 2H), 2.62 (s, 2H), 2.61 (s, 2H), 2.58 ppm (s, 2H); ^{13}C NMR (100 MHz, CD_3CN, 298 K): δ = 156.98, 140.83, 140.39, 134.98, 133.18, 131.49, 129.08, 128.89, 128.61, 128.54, 128.48, 128.28, 128.21, 127.06, 126.90, 123.71, 123.11, 122.32, 99.73, 94.05, 88.53, 79.19, 56.66, 55.33 ppm; MS (ESI): *m/z*: 1738.3830 $[Fe_2L_3-2NTf_2^-]^{2+}$, 1065.6178 $[Fe_2L_3-3NTf_2^-]^{3+}$, 729.2373 $[Fe_2L_3-4NTf_2^-]^{4+}$.

R-Cage 2: Following the general procedure, **R-Ligand 2** (28.25 mg, 0.036 mmol), $Fe(NTf_2)_2$ (14.78 mg, 0.024 mmol), and benzylamine (7.72 mg, 0.072 mmol) were added in order. **R-Cage 2** was isolated as a dark-purple solid (34.8 mg, 71%). ^{1}H NMR (400 MHz, CD_3CN, 298 K): δ = 8.57 (s, 1H), 8.56 (s, 1H), 8.51 (s, 2H), 8.48 (s, 2H), 8.28 (s, 3H), 8.26 (m, 2H), 8.16 (m, 9.0 Hz, 7H), 7.94 (m, 6H), 7.74 (d, J = 8.2 Hz, 3H), 7.61 (d, J = 8.2 Hz, 5H), 7.57–7.52 (m, 9H), 7.49 (m, 8H), 7.44 (d, J = 8.0 Hz, 7H), 7.38–7.30 (m, 12H), 7.23 (t, J = 6.9 Hz, 7H), 7.10 (m, 18H), 6.94 (d, J = 7.1 Hz, 6H), 6.86 (m, 6H), 5.52 (m, 3H), 5.48–5.37 (m, 4H), 5.09 (m, 4H), 5.04–4.79 (m, 18H), 2.50 (s, 5H), 2.37 (s, 3H), 2.35 ppm (s, 4H); ^{13}C NMR (100 MHz, CD_3CN, 298 K): δ = 174.93, 157.31, 157.21, 153.34, 153.20, 152.87, 139.91, 139.56, 137.14, 136.94, 135.83, 135.60, 134.85, 134.80, 133.08, 131.25, 129.98, 129.37, 128.78, 128.57, 128.46, 128.41, 128.30, 128.12, 128.07, 126.83, 126.73, 125.04, 122.44, 99.59, 99.47, 93.41, 89.27, 66.44, 66.21, 56.41, 56.27, 15.54 ppm; MS (ESI): *m/z*: 1780.4231 $[Fe_2L_3-2NTf_2^-]^{2+}$, 1093.6426 $[Fe_2L_3-3NTf_2^-]^{3+}$, 750.2604 $[Fe_2L_3-4NTf_2^-]^{4+}$.

RR-Cage: Following the general procedure, **R-Ligand 2** (28.24 mg, 0.036 mmol), $Fe(NTf_2)_2$ (14.78 mg, 0.024 mmol), and (*R*)-α-phenylethylamine (8.72 mg, 0.072 mmol) were added in order. **RR-Cage** was isolated as a dark-purple solid (39.4 mg, 78%). ^{1}H NMR (400 MHz, CD_3CN, 298 K): δ = 8.76 (s, 6H), 8.29 (s, 6H), 8.04 (dd, J = 8.2, 2.0 Hz, 8H), 7.95 (d, J = 8.2 Hz, 8H), 7.56–7.51 (m, 18H), 7.50–7.45 (m, 16H), 7.43–7.39 (m, 14H), 7.32 (td, J = 7.6, 6.8, 1.3 Hz, 11H), 7.13 (t, J = 7.5 Hz, 10H), 7.08 (d, J = 8.6 Hz, 8H), 7.01–6.95 (m, 23H), 6.64 (d, J = 7.7 Hz, 15H), 5.27 (d, J = 6.8 Hz, 9H), 4.97 (d, J = 5.9 Hz, 7H), 4.85 (d, J = 5.9 Hz, 7H), 3.56 (d, J = 5.9 Hz, 40H), 2.34 (s, 19H), 2.08 ppm (d, J = 1.4 Hz, 17H); ^{13}C NMR (100 MHz, CD_3CN, 298 K): δ = 171.68, 158.04, 153.36, 152.62, 140.62, 139.59, 137.19, 135.76, 135.56, 134.89, 133.13, 131.29, 130.09, 128.82, 128.67, 128.32, 127.05, 126.86, 126.77, 125.62, 125.02, 99.49, 93.40, 89.28, 70.14, 56.29, 26.62 ppm; MS (ESI): *m/z*: 1822.4760 $[Fe_2L_3-2NTf_2^-]^{2+}$, 1121.6848 $[Fe_2L_3-3NTf_2^-]^{3+}$, 771.2759 $[Fe_2L_3-4NTf_2^-]^{4+}$.

RS-Cage: Following the general procedure, **R-Ligand 2** (28.24 mg, 0.036 mmol), $Fe(NTf_2)_2$ (14.78 mg, 0.024 mmol), and (*S*)-α-phenylethylamine (8.72 mg, 0.072 mmol) were added in order. **RS-Cage** was isolated as a dark-purple solid (41.2 mg, 82%). ^{1}H NMR (400 MHz, CD_3CN, 298 K): δ = 8.84 (s, 6H), 8.27 (s, 6H), 8.03 (dd, J = 8.1, 2.0 Hz, 7H), 7.93 (d, J = 8.3 Hz, 7H), 7.59 (d, J = 8.1 Hz, 8H), 7.54 (d, J = 8.3 Hz, 12H), 7.48 (t, J = 7.6 Hz, 9H), 7.35 (d, J = 8.2 Hz, 7H), 7.32–7.27 (m, 13H), 7.14–7.07 (m, 13H), 6.99 (t, J = 7.6 Hz, 15H), 6.82 (d, J = 2.0 Hz, 6H), 6.71 (d, J = 7.7 Hz, 14H), 5.38 (d, J = 6.9 Hz, 10H), 4.95 (d, J = 5.6 Hz, 6H), 4.87 (d, J = 5.7 Hz, 7H), 2.50 (s, 18H), 2.02 ppm (d, J = 6.7 Hz, 18H); ^{13}C NMR (100 MHz, CD_3CN, 298 K): δ = 171.58, 157.93, 153.25, 153.06, 140.16, 135.61, 134.76, 133.13, 131.27, 130.13, 128.72, 128.41, 126.92, 126.67, 125.68, 125.00, 99.57, 93.27, 89.02, 70.36, 56.43, 26.56 ppm; MS (CSI): *m/z*: 1822.4760 $[Fe_2L_3-2NTf_2^-]^{2+}$, 1121.6848 $[Fe_2L_3-3NTf_2^-]^{3+}$, 771.2759 $[Fe_2L_3-4NTf_2^-]^{4+}$.

Acknowledgements

We kindly acknowledge the China Scholarship Council (CSC) and the University of Amsterdam for financial support. We would like to thank Ed Zuidinga for measuring the CSI-MS spectra and Jan Meine for assistance with the DOSY NMR spectroscopy.

Conflict of interest

The authors declare no conflict of interest.

Keywords: cage compounds · chirality · coordination modes · subcomponent assembly · supramolecular chemistry

[1] a) A. V. Davis, R. M. Yeh, K. N. Raymond, *Proc. Natl. Acad. Sci. USA* **2002**, *99*, 4793 – 4796; b) F. Hof, S. L. Craig, C. Nuckolls, J. Rebek, *Angew. Chem. Int. Ed.* **2002**, *41*, 1488 – 1508; *Angew. Chem.* **2002**, *114*, 1556 – 1578; c) J. Rebek, *Acc. Chem. Res.* **2009**, *42*, 1660 – 1668; d) B. J. Holliday, C. A. Mirkin, *Angew. Chem. Int. Ed.* **2001**, *40*, 2022 – 2043; *Angew. Chem.* **2001**, *113*, 2076 – 2097; e) M. Yoshizawa, J. K. Klosterman, M. Fujita, *Angew. Chem. Int. Ed.* **2009**, *48*, 3418 – 3438; *Angew. Chem.* **2009**, *121*, 3470 – 3490; f) S. J. Dalgarno, N. P. Power, J. L. Atwood, *Coord. Chem. Rev.* **2008**, *252*, 825 – 841; g) S. Zarra, D. M. Wood, D. A. Roberts, J. R. Nitschke, *Chem. Soc. Rev.* **2015**, *44*, 419 – 432; h) S. H. A. M. Leenders, R. Gramage-Doria, B. de Bruin, J. N. H. Reek, *Chem. Soc. Rev.* **2015**, *44*, 433 – 448; i) K. Kobayashi, M. Yamanaka, *Chem. Soc. Rev.* **2015**, *44*, 449 – 466; j) J.-N. Rebilly, B. Colasson, O. Bistri, D. Over, O. Reinaud, *Chem. Soc. Rev.* **2015**, *44*, 467 – 489; k) D. Ajami, L. Liu, J. Rebek, Jr., *Chem. Soc. Rev.* **2015**, *44*, 490 – 499; l) J. H. Jordan, B. C. Gibb, *Chem. Soc. Rev.* **2015**, *44*, 547 – 585.

[2] a) S. Leininger, B. Olenyuk, P. J. Stang, *Chem. Rev.* **2000**, *100*, 853 – 908; b) M. Fujita, M. Tominaga, A. Hori, B. Therrien, *Acc. Chem. Res.* **2005**, *38*, 369 – 378; c) R. W. Saalfrank, H. Maid, A. Scheurer, *Angew. Chem. Int. Ed.* **2008**, *47*, 8794 – 8824; *Angew. Chem.* **2008**, *120*, 8924 – 8956; d) M. D. Pluth, R. G. Bergman, K. N. Raymond, *Acc. Chem. Res.* **2009**, *42*, 1650 – 1659; e) P. Jin, S. J. Dalgarno, J. L. Atwood, *Coord. Chem. Rev.* **2010**, *254*, 1760 – 1768; f) R. Chakrabarty, P. S. Mukherjee, P. J. Stang, *Chem. Rev.* **2011**, *111*, 6810 – 6918; g) T. R. Cook, Y. R. Zheng, P. J. Stang, *Chem. Rev.* **2013**, *113*, 734 – 777; h) M. M. J. Smulders, I. A. Riddell, C. Browne, J. R. Nitschke, *Chem. Soc. Rev.* **2013**, *42*, 1728 – 1754; i) M. D. Ward, P. R. Raithby, *Chem. Soc. Rev.* **2013**, *42*, 1619 – 1636; j) M. Han, D. M. Engelhard, G. H. Clever, *Chem. Soc. Rev.* **2014**, *43*, 1848 – 1860; k) M. Raynal, P. Ballester, A. Vidal-Ferran, P. W. N. M. van Leeuwen, *Chem. Soc. Rev.* **2014**, *43*, 1734 – 1787.

[3] a) V. F. Slagt, J. N. H. Reek, P. C. J. Kamer, P. W. N. M. Van Leeuwen, *Angew. Chem. Int. Ed.* **2001**, *40*, 4271 – 4274; *Angew. Chem.* **2001**, *113*, 4401 – 4404; b) V. F. Slagt, P. C. J. Kamer, P. W. N. M. Van Leeuwen, J. N. H. Reek, *J. Am. Chem. Soc.* **2004**, *126*, 1526 – 1536; c) X. Wang, S. S. Nurttila, W. I. Dzik, R. Becker, J. Rodgers, J. N. H. Reek, *Chem. Eur. J.* **2017**, *23*, 14769 – 14777.

[4] X. Jing, Y. Yang, C. He, Z. Chang, J. N. H. Reek, C. Duan, *Angew. Chem. Int. Ed.* **2017**, *56*, 11759 – 11763; *Angew. Chem.* **2017**, *129*, 11921 – 11925.

[5] M. Kuil, T. Soltner, P. W. N. M. Van Leeuwen, J. N. H. Reek, *J. Am. Chem. Soc.* **2006**, *128*, 11344 – 11345.

[6] R. Bellini, S. H. Chikkali, G. Berthon-Gelloz, J. N. H. Reek, *Angew. Chem. Int. Ed.* **2011**, *50*, 7342 – 7345; *Angew. Chem.* **2011**, *123*, 7480 – 7483.

[7] A. Cavarzan, A. Scarso, P. Sgarbossa, G. Strukul, J. N. H. Reek, *J. Am. Chem. Soc.* **2011**, *133*, 2848 – 2851.

[8] A. C. Jans, A. Gómez-Suárez, S. P. Nolan, J. N. H. Reek, *Chem. Eur. J.* **2016**, *22*, 14836 – 14839.

[9] T. Gadzikwa, R. Bellini, H. L. Dekker, J. N. H. Reek, *J. Am. Chem. Soc.* **2012**, *134*, 2860 – 2863.

[10] R. Gramage-Doria, J. Hessels, S. H. A. M. Leenders, O. Tröppner, M. Dürr, I. Ivanović-Burmazović, J. N. H. Reek, *Angew. Chem. Int. Ed.* **2014**, *53*, 13380 – 13384; *Angew. Chem.* **2014**, *126*, 13598 – 13602.

[11] C. García-Simón, R. Gramage-Doria, S. Raoufmoghaddam, T. Parella, M. Costas, X. Ribas, J. N. H. Reek, *J. Am. Chem. Soc.* **2015**, *137*, 2680 – 2687.

[12] Q.-Q. Wang, S. Gonell, S. H. A. M. Leenders, M. Dürr, I. Ivanović-Burmazović, J. N. H. Reek, *Nat. Chem.* **2016**, *8*, 225 – 230.

[13] a) M. J. Wiester, P. A. Ulmann, C. A. Mirkin, *Angew. Chem. Int. Ed.* **2011**, *50*, 114 – 137; *Angew. Chem.* **2011**, *123*, 118 – 142; b) C. J. Brown, F. D. Toste, R. G. Bergman, K. N. Raymond, *Chem. Rev.* **2015**, *115*, 3012 – 3035; c) O. Bistri, O. Reinaud, *Org. Biomol. Chem.* **2015**, *13*, 2849 – 2865.

[14] A. J. Terpin, M. Ziegler, D. W. Johnson, K. N. Raymond, *Angew. Chem. Int. Ed.* **2001**, *40*, 157 – 160; *Angew. Chem.* **2001**, *113*, 161 – 164.

[15] a) J. Crassous, *Chem. Soc. Rev.* **2009**, *38*, 830 – 845; b) E. C. Constable, *Chem. Soc. Rev.* **2013**, *42*, 1637 – 1651; c) Y. Wang, J. Xu, Y. Wang, H. Chen, *Chem. Soc. Rev.* **2013**, *42*, 2930 – 2962; d) M. Liu, L. Zhang, T. Wang, *Chem. Rev.* **2015**, *115*, 7304 – 7397; e) L.-J. Chen, H.-B. Yang, M. Shionoya, *Chem. Soc. Rev.* **2017**, *46*, 2555 – 2576.

[16] a) J. R. Nitschke, *Acc. Chem. Res.* **2007**, *40*, 103 – 112; b) A. M. Castilla, W. J. Ramsay, J. R. Nitschke, *Acc. Chem. Res.* **2014**, *47*, 2063 – 2073.

[17] N. Ousaka, J. K. Clegg, J. R. Nitschke, *Angew. Chem. Int. Ed.* **2012**, *51*, 1464 – 1468; *Angew. Chem.* **2012**, *124*, 1493 – 1497.

[18] A. M. Castilla, N. Ousaka, R. A. Bilbeisi, E. Valeri, T. K. Ronson, J. R. Nitschke, *J. Am. Chem. Soc.* **2013**, *135*, 17999 – 18006.

[19] A. M. Castilla, M. A. Miller, J. R. Nitschke, M. M. J. Smulders, *Angew. Chem. Int. Ed.* **2016**, *55*, 10616 – 10620; *Angew. Chem.* **2016**, *128*, 10774 – 10778.

[20] a) Y. Chen, S. Yekta, A. K. Yudin, *Chem. Rev.* **2003**, *103*, 3155 – 3211; b) M. M. Pereira, M. J. F. Calvete, R. M. B. Carrilho, A. R. Abreu, *Chem. Soc. Rev.* **2013**, *42*, 6990 – 7027; c) P. Kočovský, Š. Vyskočil, M. Smrčina, *Chem. Soc. Rev.* **2003**, *103*, 3213 – 3245; d) M. Shibasaki, S. Matsunaga, *Chem. Soc. Rev.* **2006**, *35*, 269 – 279; e) L. Eberhardt, D. Armspach, J. Harrowfield, D. Matt, *Chem. Soc. Rev.* **2008**, *37*, 839 – 864; f) L. Pu, *Acc. Chem. Res.* **2014**, *47*, 1523 – 1535; g) D. Parmar, E. Sugiono, S. Raja, M. Rueping, *Chem. Rev.* **2014**, *114*, 9047 – 9153.

[21] S. J. Lee, W. Lin, *Acc. Chem. Res.* **2008**, *41*, 521 – 537.

[22] Y. Ye, T. R. Cook, S. P. Wang, J. Wu, S. Li, P. J. Stang, *J. Am. Chem. Soc.* **2015**, *137*, 11896 – 11899.

[23] J. Bunzen, T. Bruhn, G. Bringmann, A. Lützen, *J. Am. Chem. Soc.* **2009**, *131*, 3621 – 3630.

[24] a) C. Gütz, R. Hovorka, G. Schnakenburg, A. Lützen, *Chem. Eur. J.* **2013**, *19*, 10890 – 10894; b) C. Klein, C. Gütz, M. Bogner, F. Topič, K. Rissanen, A. Lützen, *Angew. Chem. Int. Ed.* **2014**, *53*, 3739 – 3742; *Angew. Chem.* **2014**, *126*, 3814 – 3817.

[25] C. Gütz, R. Hovorka, C. Klein, Q.-Q. Jiang, C. Bannwarth, M. Engeser, C. Schmuck, W. Assenmacher, W. Mader, F. Topić, K. Rissanen, S. Grimme, A. Lützen, *Angew. Chem. Int. Ed.* **2014**, *53*, 1693 – 1698; *Angew. Chem.* **2014**, *126*, 1719 – 1724.

[26] N. Struch, C. Frömbgen, G. Schnakenburg, A. Lützen, *Eur. J. Org. Chem.* **2017**, 4984 – 4989.

[27] S. E. Howson, L. E. N. Allan, N. P. Chmel, G. J. Clarkson, R. Van Gorkum, P. Scott, *Chem. Commun.* **2009**, 1727 – 1729.

[28] S. E. Howson, L. E. N. Allan, N. P. Chmel, G. J. Clarkson, R. J. Deeth, A. D. Faulkner, D. H. Simpson, P. Scott, *Dalton Trans.* **2011**, *40*, 10416 – 10433.

[29] M. C. Young, A. M. Johnson, R. J. Hooley, *Chem. Commun.* **2014**, *50*, 1378 – 1380.

[30] M. Kieffer, B. S. Pilgrim, T. K. Ronson, D. A. Roberts, M. Aleksanyan, J. R. Nitschke, *J. Am. Chem. Soc.* **2016**, *138*, 6813 – 6821.

[31] M. J. Hannon, C. L. Painting, A. Jackson, J. Hamblin, W. Errington, *Chem. Commun.* **1997**, 1807 – 1808.

[32] C. Zhao, Q. F. Sun, W. M. Hart-Cooper, A. G. Dipasquale, F. D. Toste, R. G. Bergman, K. N. Raymond, *J. Am. Chem. Soc.* **2013**, *135*, 18802 – 18805.

[33] L. L. Yan, C. H. Tan, G. L. Zhang, L. P. Zhou, J. C. Bünzli, Q. F. Sun, *J. Am. Chem. Soc.* **2015**, *137*, 8550 – 8555.

[34] C. Recsei, C. S. P. McErlean, *Tetrahedron* **2012**, *68*, 464 – 480.

[35] D. Qiu, L. Jin, Z. Zheng, H. Meng, F. Mo, X. Wang, Y. Zhang, J. Wang, *J. Org. Chem.* **2013**, *78*, 1923 – 1933.

Manuscript received: March 2, 2018
Revised manuscript received: July 16, 2018
Accepted manuscript online: July 19, 2018
Version of record online: September 6, 2018

